IEEE Access
Multidisciplinary | Rapid Review | Open Access Journal

Received 29 May 2023, accepted 14 June 2023, date of publication 19 June 2023, date of current version 19 July 2023.

Digital Object Identifier 10.1109/ACCESS.2023.3287219

RESEARCH ARTICLE

Numerical Evaluation of a Concentrated-Winding Variable Flux Memory Motor With a Hybrid Magnet Arrangement

JIN HWAN LEE[1], JUN-YOUNG SONG[2], HAN-KYEOL YEO[3], AND SANG-YONG JUNG[4], (Member, IEEE)

[1]Electric Power System Design Team, Hyundai-Transys, Hawseong-si 18280, South Korea
[2]E-Drive Materials Research Team, Hyundai Motor Company, Uiwang-si 16082, South Korea
[3]Division of Electrical & Electronic Engineering, The University of Suwon, Hwaseong-si 18323, Korea
[4]School of Electronic and Electrical Engineering, Sungkyunkwan University, Suwon-si 16419, South Korea

Corresponding author: Sang-Yong Jung (syjung@skku.edu)

ABSTRACT This paper presents a novel variable flux memory motor (VFMM) with a series–parallel configuration that employs a constant-magnetization permanent magnet (CPM) with high coercivity and a variable-magnetization permanent magnet (VPM) with low coercivity. The CPMs in the proposed VFMM are arranged in parallel. Therefore, they share an air gap. Meanwhile, the VPMs are arranged in series with respect to the CPMs, as well as each other. The CPM-induced magnetic field not only reduces the re-magnetizing current for the VPMs but also enhances the torque density. Additionally, it can assist VPMs in resisting demagnetization under loaded conditions. For verification, we compared the performance of the proposed model with that of a series-type model widely applied in VFMMs. The magnetization characteristics were investigated using nonlinear finite element analysis by deriving the VPM load line. Furthermore, the electromagnetic performance under re-magnetization and demagnetization conditions was analyzed.

INDEX TERMS Demagnetization, finite element analysis, magnetization, permanent magnet, variable flux memory motor.

I. INTRODUCTION

Permanent magnet (PM) machines have been widely used because of their high power densities and efficiencies. High-speed operation of PM machines is restricted by the voltage limit of the drive and the fixed field flux. Accordingly, a field-weakening control strategy is applied to PM machines to increase their maximum speeds. However, a negative direct-axis (d-axis) current is required to achieve field-weakening control, which results in a continuous loss. To achieve high efficiency over wide-speed operations, scholars have proposed the variable flux memory motor (VFMM). This new class of motors can control the magnetization state (MS) of the PM by applying d-axis current pulses [1], [2], [3].

The associate editor coordinating the review of this manuscript and approving it for publication was Amin Mahmoudi.

The key points to consider when designing a VFMM are as follows: 1) minimizing the magnetization current, 2) the desired range of MS control, 3) durability against demagnetization under loaded conditions, and 4) the torque density. The MS of the PM should be controllable by utilizing a limited current because a large current pulse for MS manipulation results in an oversized inverter [4], [5], [6]. Additionally, sufficient MS variation ranges should be secured to fully utilize the VFMM characteristics while satisfying the current limit of the inverter. This is generally achieved using a low-coercivity PM, referred to as a variable-magnetization PM (VPM). However, a VPM is easily demagnetized. In other words, the load current can demagnetize the VPM, limiting its maximum torque capability.

To satisfy these characteristics of VFMM, many studies have been conducted on their structural topologies [7], [8], [9], [10], [11], [12], [13]. In [7] and [8],

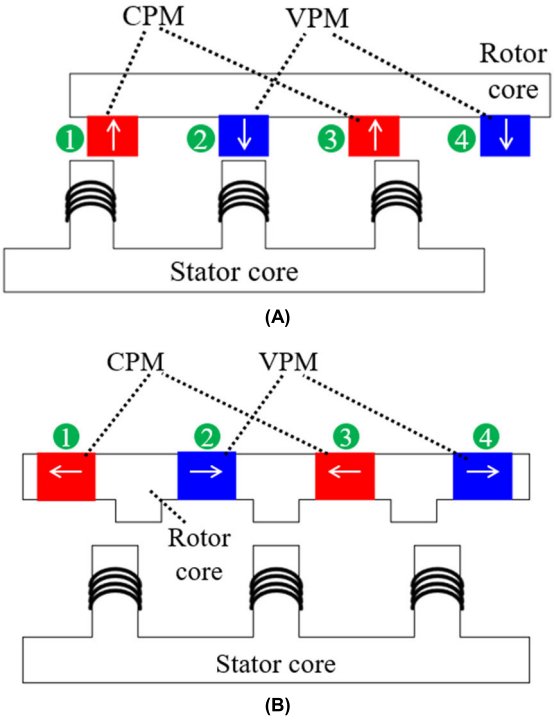

FIGURE 1. Basic configurations of a VFMM. (A) Series type. (B) Parallel type.

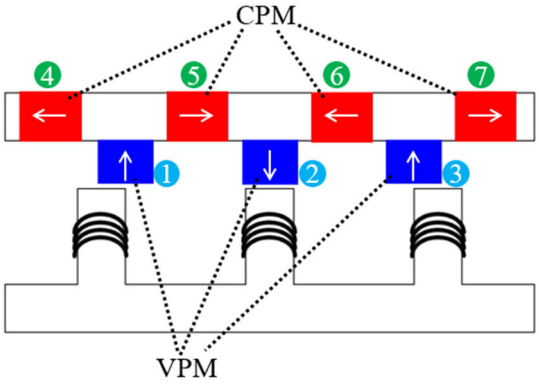

FIGURE 2. Proposed series–parallel configuration for the VFMM.

spoke-type configurations, in which PMs were magnetically connected in parallel, were employed to increase PM usage and improve torque density. However, these parallel-type VFMMs require a re-magnetizing current of at least 2.5 times the magnitude of the demagnetizing current.

These problems of the parallel type VFMMs have been overcome through various series configurations using a combination of a VPM and high-coercivity PM, which is referred to as a constant-magnetization PM (CPM) [9], [10], [11], [12], [13]. In [14], the magnetization characteristics of series and parallel configurations were studied based on an analytical method, which revealed that the series configuration is more suitable for VFMMs in terms of the re-magnetization characteristics. In other words, the re-magnetizing current required for series-type VFMMs is lower than that required for parallel-type VFMMs.

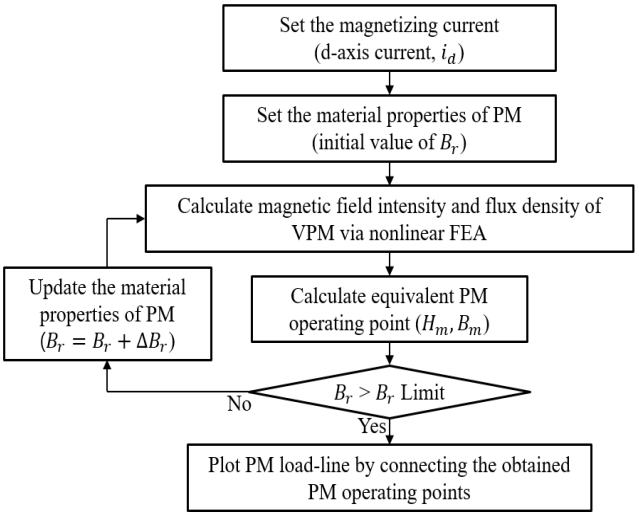

FIGURE 3. Flowchart of the numerical identification of the PM load line.

However, the series configuration still tends to require a large re-magnetizing current compared with its demagnetizing current. Accordingly, [6] and [11] adopted a method that only partially re-magnetizes the VPM instead of performing full re-magnetization. This resulted in a reduction in the MS variation range and torque density of the VFMM. This implies that additional research is required to minimize the re-magnetizing current required for VFMMs.

In this paper, a novel VFMM configuration for a washing machine with a hybrid PM arrangement is proposed. In Section II, we introduce and describe the structural characteristics of the proposed model by comparing it with relatively well-known series and parallel configurations. Section III presents the numerical methodology for plotting the PM load lines. The PM load line, an essential factor for analyzing the MS of VPMs, can be used to examine the magnetization characteristics of VFMMs. Based on this methodology, in Section IV, the magnetization characteristics are studied and compared by deriving the VPM load lines via nonlinear finite element analysis (FEA). To validate the performance of the proposed model, we compare it with a series-type VFMM that has been widely applied. The magnetization characteristics of the series and the proposed models are compared in terms of their magnetization controllability and capability. Furthermore, we performed FEA under loaded conditions to analyze durability against demagnetization and torque density issues, as described in Section V. Based on several loaded current densities, the demagnetization ratios of the VPM and output torque are calculated numerically. Finally, the torque–speed curve and efficiency maps for the two models under re-magnetization and demagnetization conditions are compared.

II. STRUCTURE OF THE VFMM

A. SERIES AND PARALLEL CONFIGURATIONS

According to previous studies, the VFMM can be divided into series and parallel magnetic circuits according to the

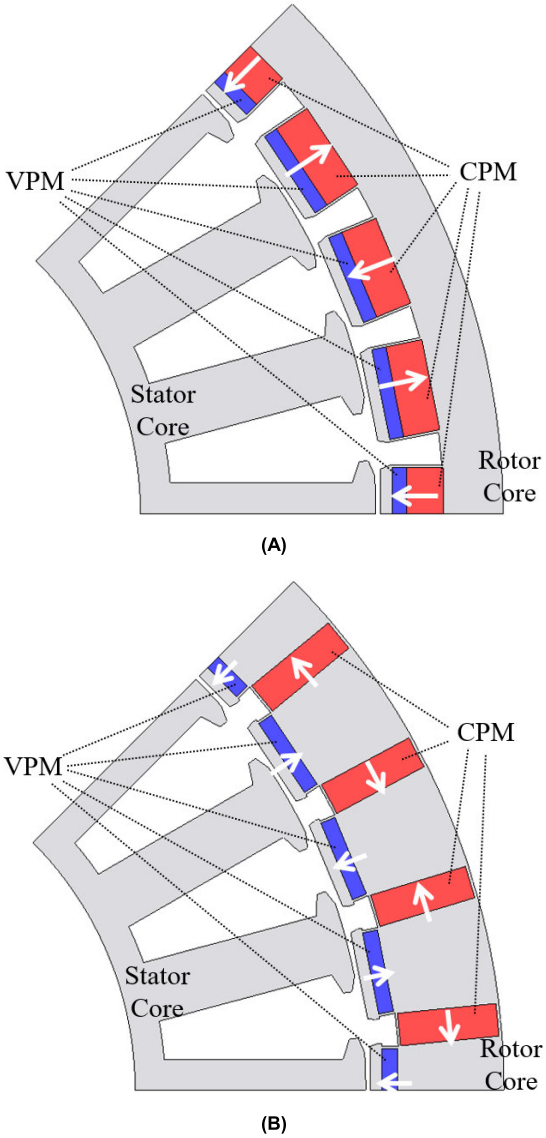

FIGURE 4. Analysis models. (A) Series VFMM. (B) Proposed VFMM.

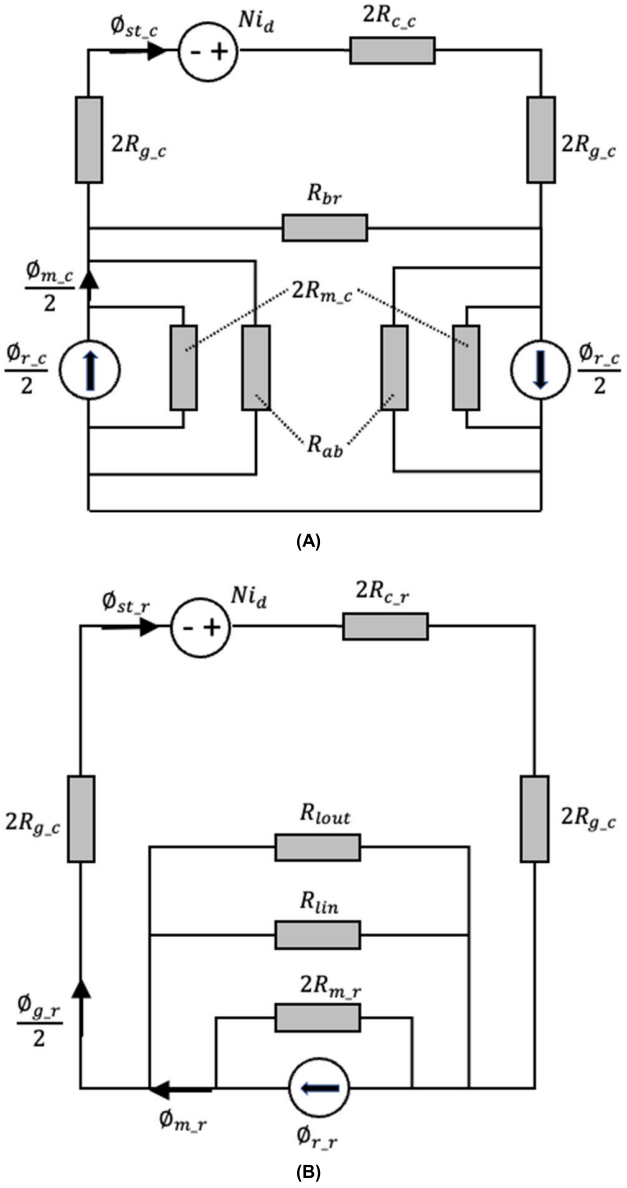

FIGURE 5. Magnetic equivalent circuit of series and parallel VFMM. (A) Series VFMM. (B) Parallel VFMM.

arrangement of the VPMs and CPMs in the rotor. If one PM occupies an air gap corresponding to a pole pitch, it is called a series configuration. In contrast, if two or more PMs share an air gap, it is called a parallel configuration. Fig. 1 presents simplified series and parallel configurations, which are four-pole/three-slot linear translation topologies, where the PMs labeled 2 and 4 are VPMs, and those labeled 1 and 3 are CPMs. For reference, a four-pole/three-slot concentrated winding VFMM was selected for this study because the external magnetic field is applied more effectively to the PM than in a two-pole/three-slot concentrated winding VFMM, as described in [11]. Meanwhile, series configurations can be further classified into two types. One has a VPM and CPM in one pole, and the other has one type of PM in one pole [4]. For reference, the series configuration shown in Fig. 1(a) is a depiction of the latter. Similarly, parallel configurations can be categorized based on the number of PMs that share an air gap.

The VPMs and CPMs shown in Fig. 1(a) are arranged in series on a magnetic circuit, whereas those shown in Fig. 1(b) are arranged in parallel. For the series configuration, the magnetic field from the CPMs is applied in the magnetization direction of the VPMs. However, this is not the case for the parallel configuration. Therefore, the external magnetic field required for re-magnetizing the VPMs in the series configuration can be reduced, compared with that in the parallel configuration, using the forward-direction magnetic field produced by the CPMs. Additionally, unexpected demagnetization of VPMs owing to inverter failure can be prevented by CPMs [8], [9]. In contrast, the VPMs and CPMs in the parallel configuration are located on the same rotor pole. Because the VPMs and CPMs share an air gap, the air-gap flux density is enhanced owing to the flux-concentrating

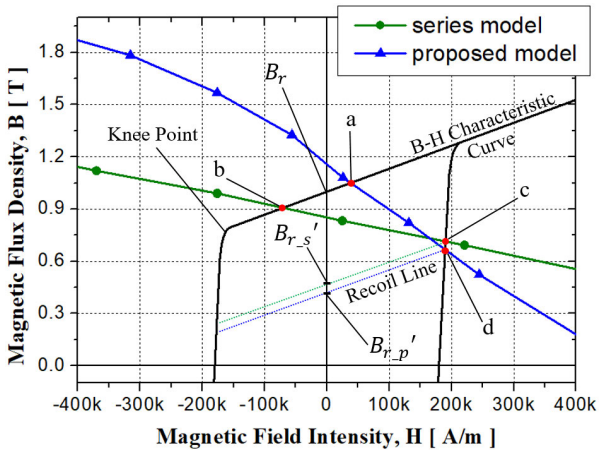

FIGURE 6. VPM load lines for series and proposed models under no-load condition.

structure. However, the magnetic field generated by CPMs affects the demagnetization characteristics of VPMs. In contrast to the series configuration, the CPM-induced magnetic fields in parallel configurations tend to demagnetize the VPMs [13].

B. SERIES AND PARALLEL CONFIGURATIONS

The series configuration has been widely applied in VFMM designs owing to the advantages described in the previous subsection. However, a large current is still required for MS manipulation, particularly for re-magnetization. The series VFMMs studied thus far require larger re-magnetizing currents than their demagnetizing currents or adopted methods that partially re-magnetize the VPM rather than performing full re-magnetization, which reduces the MS variation.

In this paper, a novel series–parallel configuration for VFMMs is introduced. The proposed configuration is shown in Fig. 2. The PMs labeled 4, 5, 6, and 7 are arranged in parallel, as shown in Fig. 1(b). In other words, the PMs share air gaps. The PMs labeled 1, 2, and 3 are arranged in series with respect to those labeled 4, 5, 6, and 7, as well as with each other. The series PM occupies an air gap corresponding to the pole pitch. Therefore, in this paper, we refer to the proposed model as a series–parallel configuration.

It should be noted that the PMs labeled 1, 2, and 3 are advantageous for re-magnetization with the aid of the forward-direction magnetic field generated by the adjacent PMs, whereas the PMs labeled 4, 5, 6, and 7 are easily demagnetized. Considering the magnetic characteristics of each PM, we utilize VPMs for the series-arranged PMs (labeled 1, 2, and 3), and CPMs for the parallel-arranged PMs (4, 5, 6, and 7). Therefore, the concentrated magnetic field generated by the radially embedded CPMs is added to the magnetization direction of the VPMs. We expect that this configuration will reduce the current required to re-magnetize the VPMs and enhance the torque density and durability against demagnetization under loaded conditions.

Meanwhile, the magnetic characteristics of the CPM-induced field are added to the VPMs in both series, and

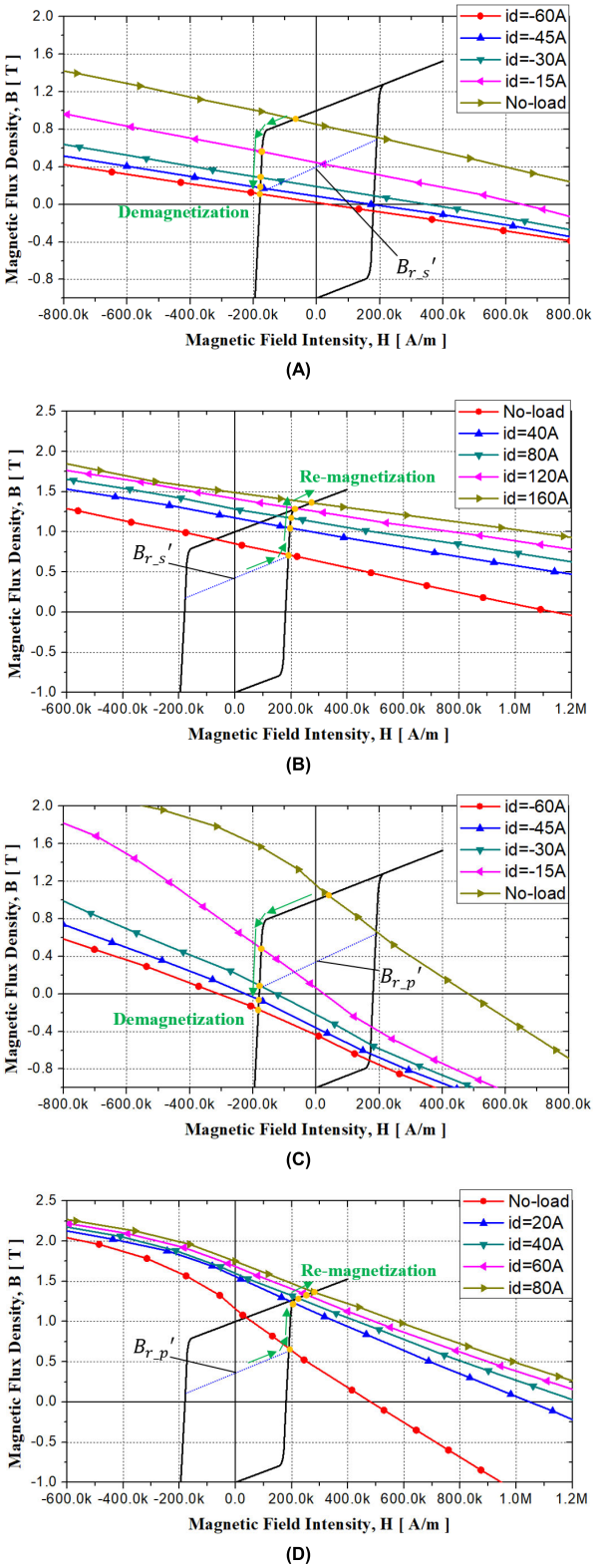

FIGURE 7. VPM load lines according to d-axis currents. (A) Series VFMM (negative d-axis current). (B) Series VFMM (positive d-axis current). (C) Proposed VFMM (negative d-axis current). (D) Proposed VFMM (positive d-axis current).

the proposed configuration may be advantageous for VFMM design in general, but it may also be disadvantageous

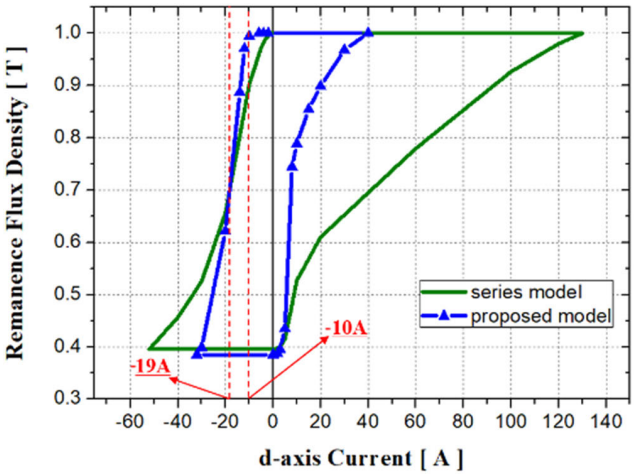

FIGURE 8. Comparison of re-magnetization and demagnetization characteristics according to d-axis currents.

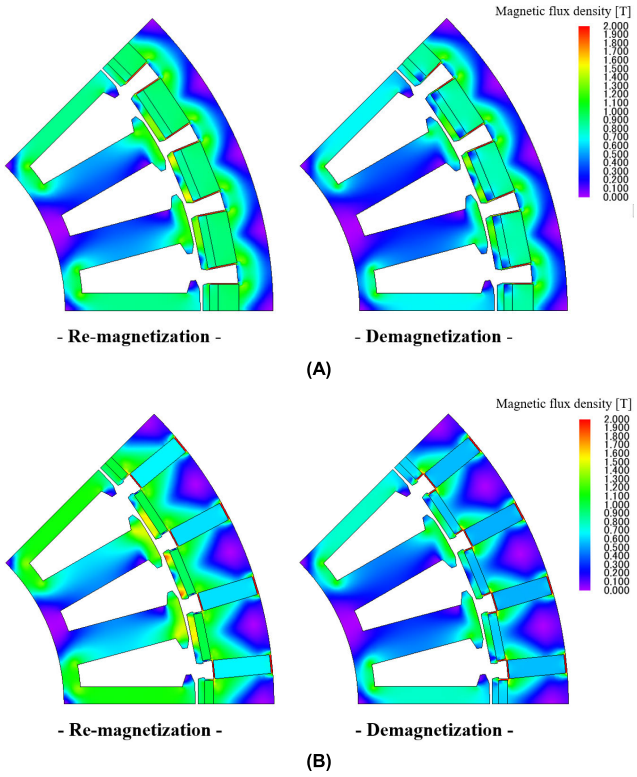

FIGURE 9. Contour plots of magnetic flux density under re-magnetization and demagnetization conditions. (A) Series VFMM. (B) Proposed VFMM.

in specific circumstances. The minimum remanence flux density of a demagnetized VPM may be restricted by the CPM-induced field. If the forward-direction magnetic field induced by the CPM is excessively large, the VPM MS manipulation range becomes narrow, which means that it may not fully utilize the characteristics of the VFMM. Additionally, the current required to demagnetize the VPM may increase because of the interference of the large CPM-induced magnetic field. Accordingly, when designing series or the proposed series–parallel VFMMs, the no-load

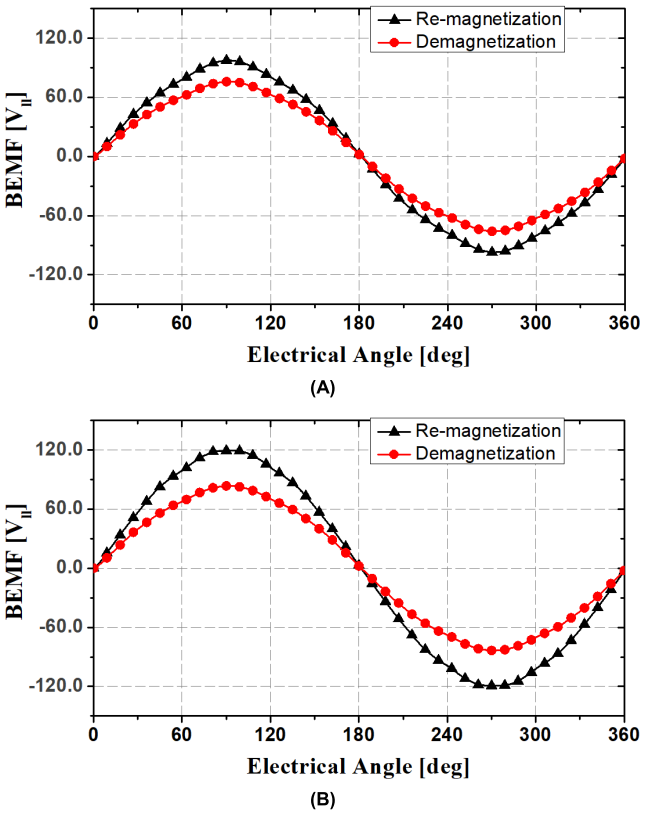

FIGURE 10. BEMFs under re-magnetization and demagnetization conditions. (A) Series type VFMM. (B) Proposed VFMM.

re-magnetization of VPMs caused by CPMs should be considered. These issues are detailed in Section IV based on VPM load lines.

III. NUMERICAL METHODOLOGY FOR DERIVING PM LOAD LINES

A. ASSUMPTIONS

Generally, the magnetic field intensity and flux density of a PM calculated using FEA differ for each element in the PM. To simplify this computation, we consider the magnetic field intensity and flux density values for all elements in the PM to be average values; thus, the PM operation can be expressed as a point.

When an armature current is applied to the motor, the PM operating point varies dynamically by following minor hysteresis loops, which are thin and have a slope virtually equal to that of the recoil line. In practice, for most PMs utilized in motors, except for the alnico alloy PM, the demagnetization curve is generally approximated as a straight line. Therefore, in this paper, a piecewise-linear hysteresis model is employed to derive the PM load lines [15].

B. PM OPERATING POINT

The PM operating point can be obtained by investigating the magnetic field intensity (H) and flux density (B) for all the elements in the PM. By calculating the average

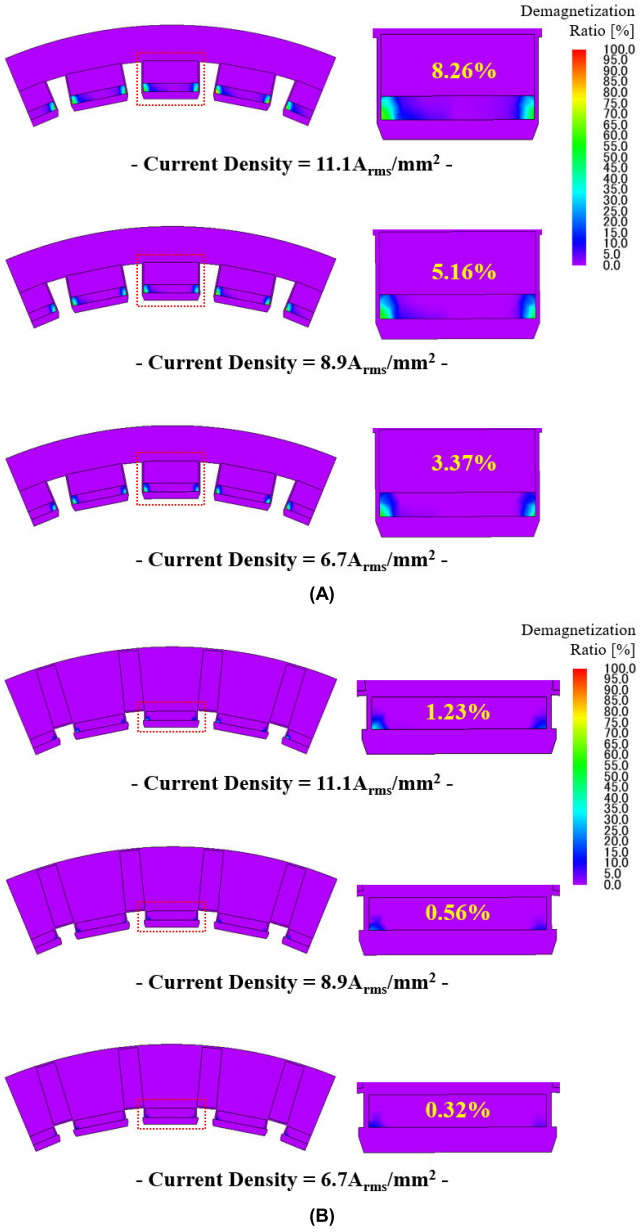

FIGURE 11. Demagnetization ratio contour plots according to overload currents. (A) Series VFMM. (B) Proposed VFMM.

values of the magnetic field intensities and flux densities in the magnetization direction, the PM operating point can be equivalently expressed as a point (H_m, B_m) as follows:

$$H_m = \sum_n [H_{x,n} \times \cos\theta + H_{y,n} \times sin\theta]/_N \quad (1)$$

$$B_m = \sum_n [B_{x,n} \times \cos\theta + B_{y,n} \times sin\theta]/_N. \quad (2)$$

H_x and B_x are the x-axis directional components, and H_y and B_y are the y-axis directional components. θ is the magnetization angle, and N is the number of elements in the PM.

C. PM LOAD LINE

Theoretically, the PM operating point is the intersection point of the PM load line and B–H characteristic curve of the PM. Hence, the PM load line can be inversely derived as connecting the calculated PM operating points according to different values of remanence flux density to B_r, which have regular intervals [11]. The entire process of plotting the PM load line via FEA is summarized in the flowchart in Fig. 3.

The magnetization characteristics can be studied in detail by identifying the slope of the derived the PM load line and position of the PM operating point. The slope of the PM load line is referred to as the permeance coefficient (PC). If a d-axis current pulse for the MS control is supplied by

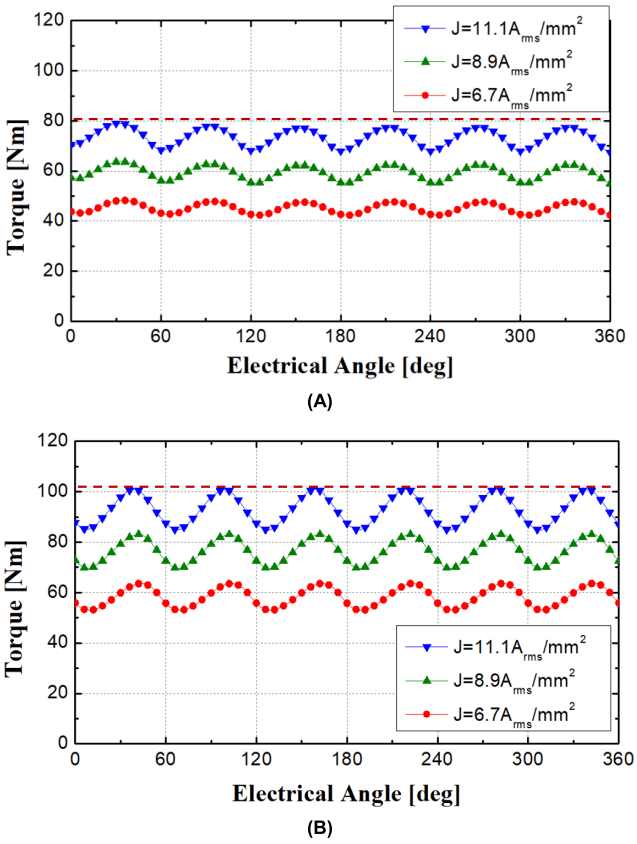

FIGURE 12. Output torque according to overload currents. (A) Series VFMM. (B) Proposed VFMM.

TABLE 1. Specifications of analysis models.

Item	Value	
Number of poles / slots	32 / 24	
Outer diameter of motor	247 mm	
Axial length of motor	40 mm	
Air-gap length	0.8 mm	
Slot fill factor	40%	
Saliency ratio	1.0	
Rated current density	6.7 A$_{rms}$/mm^2	
PM type	SmCo (VPM)	NdFeB (CPM)
PM surface area (1EA)	36.9 mm^2	95.3 mm^2
PM remanence flux density	1.0 T	
PM coercive force	180 kA/m	758 kA/m

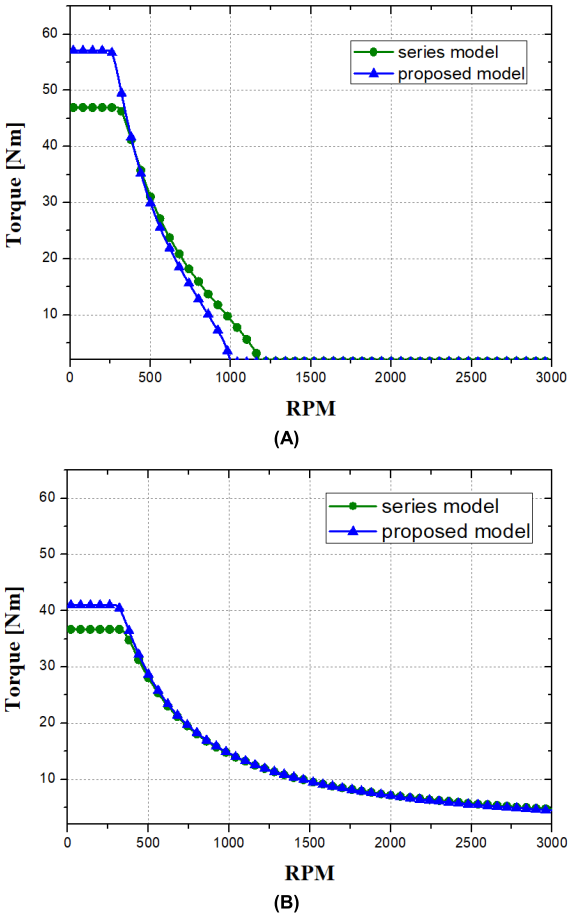

FIGURE 13. Comparison of torque–speed curves. (A) Re-magnetization state. (B) Demagnetization state.

an inverter, the PM load line is shifted, resulting in a change in the PM operating point.

IV. COMPARISON OF MAGNETIC CHARACTERISTICS

A. ANALYSIS MODELS AND MAGNETIZATION PROCESS

Fractional-slot concentrated winding motors for the series and proposed VFMMs were designed and analyzed in this study. The analysis models are presented in Fig. 4, in which the magnetization directions are indicated by arrows. Table 1 lists the specifications of the analytical models. Because the numbers of poles and slots were 32 and 24, respectively, FEA was performed using an electrical one-period model, as shown in Fig. 4. For a fair comparison, we employed identical stator and PM usage for the series and proposed VFMMs.

There are two types of re-magnetization and demagnetization processes: three-phase and two-phase excitation. In this study, we employed a three-phase excitation topology for the series and proposed VFMMs. To re-magnetize or demagnetize all the VPMs in both models, the magnetization current must flow four times in total. The input times for the magnetization currents are when the electrical angular positions of the rotor are 60°, 120°, 180°, and 240°.

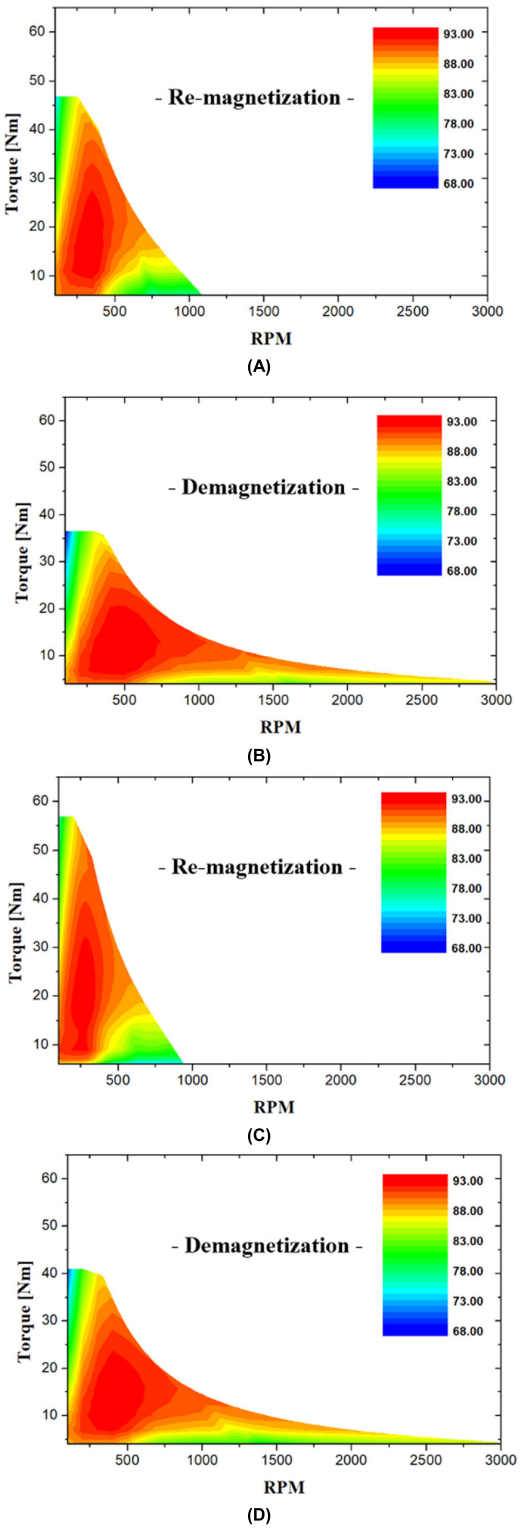

FIGURE 14. Efficiency maps. (A) Series VFMM under re-magnetized state. (B) Series VFMM under demagnetization state. (C) Proposed VFMM under re-magnetized state. (D) Proposed VFMM under demagnetized state.

B. MAGNETIC EQUIVALENT CIRCUIT ANALYSIS FOR THE MODELS

Before the FEA, a magnetic equivalent circuit (MEC) was constructed using an analytical method. As previously

assumed, the calculation was performed using the average value of the magnetic flux density and magnetic field in the PM to simplify the calculation. During magnetizing and demagnetizing control, the modeling of the rotor magnetic steel sheet can be omitted because the main magnetic path is not saturated. However, the modeling of the rotor bridge was considered to account for magnetic flux leakage. However, because magnetic saturation occurs more severely in the stator magnetic steel sheet than in the rotor, all reluctances were calculated and reflected in the modeling.

Fig. 5 shows the magnetic equivalent circuit constructed by calculating the magnetic circuit considering the above conditions.

Here, each parameter is described as follows.

- ϕ_r: Magnetic flux source of a PM pole.
- ϕ_m: Magnetic flux flowing in the PM.
- ϕ_{st}: Magnetic flux flowing through the stator teeth.
- R_g: Reluctance of the air gap.
- R_m: Reluctance of the PM.
- R_{br}: Reluctance of the rotor's bridge in the series VFMM.
- R_{ab}: Reluctance of the rotor's air barrier in the series VFMM.
- R_{lin}: Rotor internal leakage reluctance of the parallel VFMM.
- R_{lout}: Rotor outer leakage reluctance of the parallel VFMM.
- R_c: Reluctance of the stator teeth and yoke.

As shown in Fig. 5, MECs were constructed, and they were used for preliminary analysis. Because the VFMM has the characteristic of severe magnetic saturation during the magnetizing and demagnetizing processes, a detailed analysis was performed using FEA.

C. VPM LOAD LINES FOR MAGNETIZATION CHARACTERISTICS INVESTIGATION

To investigate the magnetization characteristics, we derived the VPM load lines for the analysis models via nonlinear FEA based on the numerical methodology described in Section III. Fig. 6 shows the VPM load lines under the no-load condition, where the circular and triangular lines represent the load lines for the series and proposed models, respectively. Points a and b in Fig. 6 are the no-load VPM operating points, which are the intersection points between the load lines and B–H characteristic curve of the VPM.

Generally, a no-load PM line has a negative PC that passes through the origin of the B–H characteristic curve of the PM. Therefore, the no-load PM operating point is positioned in the second quadrant because all PM motors have an air gap in their magnetic circuits. However, the VPM load lines for the series and proposed VFMMs do not cross the origin, as shown in Fig. 6, primarily because of the forward magnetic field generated by the CPMs.

Furthermore, the VPM operating point of the proposed model (point a in Fig. 6) is in the first quadrant through the CPMs, whereas the operating point of the series model (point b) is in the second quadrant. This indicates that the VPMs in the proposed model are significantly more affected by the CPM-induced magnetic field than those in the series model.

Although a CPM-induced magnetic field is advantageous for decreasing the required re-magnetizing current, it can limit the MS manipulation range of the VPM. Even if the VPM is demagnetized by a negative d-axis current that is sufficiently large to decrease the remanence flux density below B'_{r_s} or B'_{r_p} in Fig. 6, the VPM operating points return to points c and d under no-load conditions because of the CPM-induced magnetic field. This indicates that the reduced remanence flux density returns to B'_{r_s} or B'_{r_p}. Additionally, the controllable minimum remanence flux densities of the VPMs in the series and proposed models are B'_{r_s} and B'_{r_p}, respectively. Meanwhile, we observe from Fig. 6 that B'_{r_p} is smaller than B'_{r_s}, which is primarily owing to the lower PC of the VPM load line of the proposed model compared with that of the series model.

We confirmed the magnitude of the demagnetizing current required to decrease B_r to its minimum value (B'_{r_s} or B'_{r_p}) by investigating the VPM load lines associated with negative d-axis currents. Additionally, the load lines associated with positive d-axis currents were derived to identify the current required to fully re-magnetize the VPM. Fig. 7 shows a comparison of the VPM load lines of the two models. The re-magnetization and demagnetization characteristics associated with the d-axis currents are shown in Fig. 8. The re-magnetizing currents for the series and proposed models were 130 and 40 A, and the demagnetizing currents were −52 and −32 A, respectively.

When the negative d-axis current was less than −19 A, the VPM in the series model demagnetized more easily than that in the proposed model, as shown in Fig. 8. However, when the current was larger than −19 A, the VPM in the proposed model demagnetized more easily. The fact that the proposed model requires a smaller demagnetizing current but has better demagnetization durability under low-current conditions indicates that it is superior to the series model in terms of magnetization controllability and durability against unintentional demagnetization.

D. COMPARISON OF NO-LOAD CHARACTERISTICS

To analyze the effectiveness of the variable MS characteristics in detail, we calculated the back electromotive force (BEMF) via FEA with the VPM properties under re-magnetization and demagnetization conditions. The no-load magnetic flux density contour plots with B_r, B_(r_s)', and B_(r_p)', which are necessary for the BEMF calculations, are presented in Fig. 9. The flux generated by the CPMs easily passes through the VPMs in their re-magnetized state. We confirmed that the resultant magnetic flux densities in the re-magnetized state were higher than those in the demagnetized state, as shown in Fig. 9.

TABLE 2. Comparison of re-magnetization and demagnetization characteristics.

	Series VFMM	Proposed VFMM
Re-magnetization current	130 A	40 A
Demagnetization current	-52 A	-32 A
MS range	0.395–1.0 T	0.385–1.0 T
BEMF range	52.2–66.9 V_{rms}	57.8–84.0 V_{rms}
Reduction ratio of BEMF	21.9%	31.2%

The BEMFs of the two models are shown in Fig. 10. For the series VFMM, the BEMF in the re-magnetized state was 66.9 V_{rms}, and that in the demagnetized state was 52.2 V_{rms}.

The reduction rate of the BEMF as a result of MS manipulation was 21.9%. For the proposed VFMM, the BEMFs in the re-magnetized and demagnetized states were 84.0 and 57.8 V_{rms}, respectively. The reduction rate of the BEMF was 31.2%.

Table 2 summarizes the comparison of the magnetization characteristics and no-load analysis results of the series and proposed VFMMs. The proposed VFMM demonstrated superiority in terms of magnetization controllability and capability compared with the series VFMM. The demagnetizing and re-magnetizing currents for the proposed model were smaller than those for the series model. Additionally, the BEMF variation range of the proposed model was wider than that of the series model, indicating that it utilized the VFMM characteristics better.

V. COMPARISON OF LOAD CHARACTERISTICS

A. LOAD DEMAGNETIZATION AND TORQUE DENSITY

As mentioned previously, the VPM is used in VFMM designs to control the MS with a limited current from the inverter. However, a VPM can be easily demagnetized under loaded conditions because of its low coercive force, which results in torque performance degradation. In this section, the load demagnetizations of the VPMs in the two models under various load conditions are analyzed and compared.

Additionally, the torque densities of the series and proposed models were calculated by determining the peak torque after demagnetization using the load currents. As the saliency ratio of the series and proposed models was 1.0, as shown in Table 1, FEA under loaded conditions was performed with only the q-axis currents engaged to examine the load characteristics. Although the rated current density of the analysis models was 6.7 A_{rms}/mm^2, an overload current was applied to the series and proposed VFMMs to examine their durability against unintentional demagnetization. The demagnetization ratio of a VPM can be obtained by calculating the PM operating points for each element under loaded conditions based on the piecewise-linear hysteresis model. The applied overload current densities were 6.7, 8.9, and 11.1 A_{rms}/mm^2. The calculated demagnetization-ratio contour plots for the two models are shown in Fig. 11. The average demagnetization ratios specified in Fig. 11 are the average values for all the elements in the VPM. It should be noted that the VPM of the proposed model was demagnetized by 1.23% under the largest current density condition (11.1 A_{rms}/mm^2), whereas that of the series model was demagnetized by 8.26%. Thus, the proposed model had better durability against load demagnetization than the series VFMM.

TABLE 3. Comparison of key-performance index.

	Series VFMM	Proposed VFMM
Re-magnetization current	130 A	40 A
Demagnetization current	-52 A	-32 A
MS range	0.395–1.0 T	0.385–1.0 T
BEMF range	52.2–66.9 V_{rms}	57.8–84.0 V_{rms}
Reduction ratio of BEMF	21.9%	31.2%
Maximum Torque	47.2 Nm	58.1 Nm
Maximum Speed	Over 3000 rpm	

Fig. 12 shows the output torque waveforms for the two models according to the load current densities. When the highest current density (11.1 A_{rms}/mm^2) was applied, the output torque of the series model decreased gradually as it rotated, as shown in Fig. 12(a).

This was primarily caused by the demagnetization of the VPM under overload conditions, resulting in a decrease in the torque density and MS variation range. In contrast, the proposed model could better withstand the overload demagnetization. To compare the performances of the series and proposed VFMMs, we calculated the torque per load current density, because the total volumes of both models were identical, as mentioned previously. Here, the torque was obtained via nonlinear FEA with the demagnetized VPM material properties after applying the largest load current density (11.1 A_{rms}/mm^2). The calculated torque densities of the series and proposed VFMMs were 7.0 and 8.7 Nm/A_{rms}, respectively.

B. TORQUE–SPEED CURVE AND EFFICIENCY MAP

It is possible to not only improve the efficiency but also extend the maximum speed by adjusting the MS of the VPM. To investigate these metrics, we predicted torque–speed curves and efficiency maps under re-magnetized and demagnetized states through FEA simulations. Fig. 13 presents the torque–speed curves under the rated current density (6.7 A_{rms}/mm^2) and voltage (360 V) conditions, considering the copper, iron, and PM eddy current losses. The simulated efficiency maps are shown in Fig. 14.

Under the re-magnetized conditions, the maximum torque of the proposed model was larger than that of the series model. Furthermore, the proposed model achieved high efficiency in low-speed and high-torque areas. The maximum speed of the proposed model in the re-magnetized state was 1,000 rpm, whereas that of the series model was 1,180 rpm. However, this can be overcome using MS control. The maximum speed for both models can be extended to 3000 rpm by reducing the MS of the VPM. Additionally, the high-efficiency region shifted to higher speeds with the demagnetized VPM. This was because the flux linkage of the armature coil and the iron loss, which were dominant in the high-speed area, were reduced.

VI. CONCLUSION

This paper introduces a novel series–parallel configuration that is suitable for VFMMs. The structural characteristics of the proposed VFMM are introduced and described by comparison with well-known series and parallel configurations. Before analyzing the series–parallel VFMM, a numerical methodology for deriving the PM load line via FEA is described, which is an essential factor for examining the magnetization characteristics of VFMMs. To verify the performance of the proposed series–parallel configuration, we analyze a series-type VFMM and the proposed VFMM. To compare the magnetization characteristics, we derive the PM load lines under no-load and d-axis current conditions for both models. From FEA results, we confirmed that the proposed VFMM was superior to the series VFMM in terms of magnetization controllability and MS manipulation range owing to its structural characteristics. Table 3 summarizes the key performance of these models.

Furthermore, FEA was performed under load current input conditions to investigate and compare the load characteristics. The proposed VFMM demonstrated superiority in terms of torque density and durability against loaded demagnetization compared with the series-type VFMM.

REFERENCES

[1] V. Ostovic, "Memory motors," *IEEE Ind. Appl. Mag.*, vol. 9, no. 1, pp. 52–61, Jan. 2003.

[2] H. Yang, R. Tu, H. Lin, S. Niu, and S. Lyu, "Investigation of balanced bidirectional-magnetization effect of a novel hybrid-magnet-circuit variable-flux memory machine," *IEEE Trans. Magn.*, vol. 58, no. 2, pp. 1–6, Feb. 2022.

[3] R. Tsunata, M. Takemoto, S. Ogasawara, and K. Orikawa, "Variable flux memory motor employing double-layer delta-type PM arrangement and large flux barrier for traction applications," *IEEE Trans. Ind. Appl.*, vol. 57, no. 4, pp. 3545–3561, Jul. 2021.

[4] A. Athavale, K. Sasaki, B. S. Gagas, T. Kato, and R. D. Lorenz, "Variable flux permanent magnet synchronous machine (VF-PMSM) design methodologies to meet electric vehicle traction requirements with reduced losses," *IEEE Trans. Ind. Appl.*, vol. 53, no. 5, pp. 4318–4326, Sep. 2017.

[5] H. Yang, H. Zheng, H. Lin, Z. Zhu, W. Fu, W. Liu, J. Lei, and S. Lyu, "Investigation of hybrid-magnet-circuit variable flux memory machines with different hybrid magnet configurations," *IEEE Trans. Ind. Appl.*, vol. 57, no. 1, pp. 340–351, Jan. 2021.

[6] Y. Xie, Z. Ning, and Z. Ma, "Comparative study on variable flux memory machines with different arrangements of permanent magnets," *IEEE Access*, vol. 8, pp. 164304–164312, 2020.

[7] J. Jang, M. Humza, and B. Kim, "Design of a variable-flux permanent-magnet synchronous motor for adjustable-speed operation," *IEEE Trans. Ind. Appl.*, vol. 52, no. 4, pp. 2996–3004, Jul. 2016.

[8] M. Ibrahim, L. Masisi, and P. Pillay, "Design of variable-flux permanent-magnet machines using alnico magnets," *IEEE Trans. Ind. Appl.*, vol. 51, no. 6, pp. 4482–4491, Nov. 2015.

[9] N. Limsuwan, T. Kato, K. Akatsu, and R. D. Lorenz, "Design and evaluation of a variable-flux flux-intensifying interior permanent-magnet machine," *IEEE Trans. Ind. Appl.*, vol. 50, no. 2, pp. 1015–1024, Mar. 2014.

[10] T. Kato, N. Limsuwan, C. Yu, K. Akatsu, and R. D. Lorenz, "Rare earth reduction using a novel variable magnetomotive force flux-intensified IPM machine," *IEEE Trans. Ind. Appl.*, vol. 50, no. 3, pp. 1748–1756, May 2014.

[11] S. Maekawa, K. Yuki, M. Matsushita, I. Nitta, Y. Hasegawa, T. Shiga, T. Hosoito, K. Nagai, and H. Kubota, "Study of the magnetization method suitable for fractional-slot concentrated-winding variable magnetomotive-force memory motor," *IEEE Trans. Power Electron.*, vol. 29, no. 9, pp. 4877–4887, Sep. 2014.

[12] J. Kim, D. Kim, G. Park, Y. Kim, and S. Jung, "Analysis and design of SPM type variable flux memory motor considering demagnetization characteristic of permanent magnet," *IEEE Trans. Appl. Supercond.*, vol. 28, no. 3, pp. 1–5, Apr. 2018.

[13] H. Hua, Z. Q. Zhu, A. Pride, R. P. Deodhar, and T. Sasaki, "A novel variable flux memory machine with series hybrid magnets," *IEEE Trans. Ind. Appl.*, vol. 53, no. 5, pp. 4396–4405, Sep. 2017.

[14] J. Song, J. H. Lee, D. Kim, Y. Kim, and S. Jung, "Analysis and modeling of permanent magnet variable flux memory motors using magnetic equivalent circuit method," *IEEE Trans. Magn.*, vol. 53, no. 11, pp. 1–5, Nov. 2017.

[15] X. Zhu, L. Quan, D. Chen, M. Cheng, W. Hua, and X. Sun, "Electromagnetic performance analysis of a new stator-permanent-magnet doubly salient flux memory motor using a piecewise-linear hysteresis model," *IEEE Trans. Magn.*, vol. 47, no. 5, pp. 1106–1109, May 2011.

JIN HWAN LEE was born in Goesan, South Korea, in 1986. He received the B.S. and Ph.D. degrees in electronic and electrical engineering from Sungkyunkwan University, Suwon, South Korea, in 2013 and 2018, respectively.

He is currently a Senior Research Engineer with the Research and Development Division, Hyundai-Transys. His research interests include the numerical analysis and design optimization of electric machines and the development of optimization algorithm.

JUN-YOUNG SONG was born in Cheongju, South Korea, in 1989. He received the B.S. and Ph.D. degrees in electronic and electrical engineering from Sungkyunkwan University, Suwon, South Korea, in 2014, and 2019, respectively.

He is currently a Research Engineer with the Research and Development Division, LG Electronics. His research interest includes the analytical and numerical analysis of electric machines.

HAN-KYEOL YEO received the B.S. degree in electronic and electrical engineering from Sungkyunkwan University, Suwon, South Korea, in 2012, and the Ph.D. degree (combined master's and Ph.D. program) in electrical engineering from Seoul National University, Seoul, South Korea, in 2018.

From 2018 to 2021, he was a Senior Research Engineer with the Advanced Electrification Development Team, Hyundai Motor Company, Hwaseong, South Korea. He is currently an Assistant Professor with the Division of Electrical and Electronic Engineering, Suwon University, Hwaseong. His research interest includes the analysis and optimal design of electric machines.

SANG-YONG JUNG (Member, IEEE) received the B.S., M.S., and Ph.D. degrees in electrical engineering from Seoul National University, Seoul, South Korea, in 1997, 1999, and 2003, respectively.

From 2003 to 2006, he was a Senior Research Engineer with the Research and Development Division, Hyundai Motor Company, Seoul, and the Research and Development Division, Kia Motor, Seoul. He is currently a Professor with the School of Electronic and Electrical Engineering, Sungkyunkwan University, Suwon, South Korea. His research interests include the numerical analysis and optimal design of electric machines and power apparatus.